Ab-initio determination of high pressure and high temperature thermoelastic and thermodynamic properties of low-spin $(Mg_{1-X}Fe_X)O$ ferropericlase with x in the range [0.06, 0.59]

Isacco Scanavino and Mauro Prencipe

Isacco Scanavino (*) and Mauro Prencipe
Dipartimento di Scienze della Terra,
Università di Torino, Via Valperga Caluso 35,
10125 Torino, Italy
* E-mail: isacco.scanavino@libero.it

Abstract

In this work we calculate the thermo-elastic properties of $(Mg_{1-x}Fe_x)O$ ferropericlase, with x in the [0.06, 0.59] range, and the thermodynamic properties of ferropericlase having the specific stoichiometric composition $(Mg_{0.54}Fe_{0.46})O$, at pressures and temperatures which are those typical of the Earth's lower mantle. We follow an *ab-initio* quantum-mechanical approach, with the use of the WC1LYP hybrid HF/DFT (Hartree-Fock/Density Functional Theory) functional, within the framework of the quasi-harmonic approximation. Iron is assumed to be in the low spin configuration, as it proved to be the most stable spin arrangement at the thermo-baric conditions of the deepest lower mantle. The choice of the low spin configuration, and the use of an *ab-initio* approach, make this work unique as it

is the first time that such a technique is applied for the calculation of the vibrational and thermodynamic properties of the low spin ferropericlase.

We observe a linear increase of the bulk modulus and a linear decrease of the cell volume as iron content increases. More precisely, for x = 0.46, at ambient condition K_T = 205.57 GPa, K'_T = 4.242 and V_T = 72.216 Å^3; for x = 0.03, at the same conditions, K_T = 167.42 GPa, K'_T = 4.085 and V_T = 75.145 Å^3. Some thermodynamic parameters and the thermal expansion (C_V, C_P, S, α) for $(Mg_{0.54}Fe_{0.46})O$ are calculated both at ambient condition [C_V = 36.11 J/(mole*K), C_P = 36.38 J/(mole*K), S = 26.62 J/(mole*K), α = 1.97*10^{-5} K^{-1}], and at simultaneous high-pressure and high-temperature conditions as a function of the geobar and geotherm curves. The data here proposed can be seen as possible bounds to the values of thermoelastic and thermodynamic parameters employed in the construction of geophysical models and the same data could be used to revise the velocity of the seismic waves in the lower mantle.

Keywords Ferropericlase, lower mantle, thermoelastic properties, thermodynamic properties

Introduction

The magnesium-rich $(Mg_x,Fe_{1-x})O$ solid solution, known as the mineral ferropericlase, constitutes a significant part of the Earth, as it is the second most abundant mineral in the lower mantle (660 – 2890 km depth) following $(Mg,Fe)SiO_3$ perovskite (Irifune 1994; Wood 2000). Its structure (the rock-salt one; space group *Fm-3m*), is stable across the whole lower mantle depth range (Fei et al. 1992; Lin et al. 2003), so that the knowledge of its elastic properties at high-pressure (HP) and high-temperature (HT) as a function of the iron content is of crucial importance for the geophysics of the mantle. To the authors' knowledge, in spite of the great importance of this phase, only a few experimental

68 measurements at lower mantle pressure conditions do exist and they mainly address three topics: (i) the
69 prediction of the high-spin (HS) low-spin (LS) transition (Jacobsen et al. 2002; Lin et al. 2003, 2005;
70 Speziale et al. 2005; Lin et al. 2006; Tsuchiya et al. 2006; Fei et al. 2007; Lin et al. 2007; Komabayashi
71 et al. 2010); (ii) the measurement of the elastic properties up to HP conditions (Fei et al. 1992; Fei
72 1999; Kung et al. 2002; J. Zhang and Kostak 2002; van Westrenen et al. 2005; Jackson et al. 2006;
73 Speziale et al. 2007; Fei et al. 2007; Crowhurst et al. 2008; Reichmann, Sinogeikin, and Bass 2008;
74 Komabayashi et al. 2010; Matsui et al. 2012); and (iii) the determination of the possible phase
75 transitions in the lower mantle (H.K. Mao, Shen, and Hemley 1997; Wood 2000). Of these
76 experimental works, only a few deal in detail with ferropericlase in its low-spin configuration (Chen et
77 al., 2012; Fei et al., 2007; Lin et al., 2005; Mao et al., 2011; Speziale et al., 2007). Regarding the
78 computational works, although they have demonstrated to be able to correctly predict the elastic
79 properties of oxides and silicates at simultaneous HP/HT conditions (Oganov, Brodholt, and Price
80 2002; Ottonello et al. 2010; Scanavino et al. 2012) and, at the same time, to predict the correct spin
81 states of iron through the use of appropriate methodologies, by using spin polarized Hamiltonians
82 (Pisani 1996), there are only few papers focused on the ferropericlase with iron in LS configuration
83 (Persson et al. 2006; Scanavino et al. 2012; Wentzcovitch et al. 2009; Wu et al. 2009).
84 The choice of the spin state of iron in ferropericlase is extremely important as the two different states
85 are stable at different P/T conditions and consequently at different depth in the Earth's interior. It is
86 known that the spin configuration of the iron in ferropericlase is strictly dependent on the temperature
87 and on the iron concentration: in particular, it is known that the increase of temperature shifts the spin
88 transition to higher pressures [from 50 GPa at 300 K, to 70 GPa at 2000 K for the $(Mg_{0.75}Fe_{0.25})O$
89 composition (Lin et al. 2007)] and that the increase of the iron content shifts the transition towards
90 higher pressures [from 30 GPa at room temperature for ferropericlase having a small amount of iron,
91 up to 90 GPa for wustite (Speziale et al. 2005)]. The determination of the high-spin to low- spin

crossover region is still controversial as it occurs over a very broad pressure region at typical lower mantle temperatures (Kantor et al. 2009, Lin and Tsuchiya 2008,Sturnhahn et al. 2005, Wentzcovitch et al. 2009) and also because the experimental observation in wustite is highly controversial (Badro et al. 1999, Pasternak et al. 1997).

In this work, following an *ab-initio* quantum-mechanical approach within the framework of the quasi-harmonic approximation (QHA), we aim to calculate the elastic properties of ferropericlase having composition in the range from $(Mg_{0.94}Fe_{0.06})O$ [FeO content 8.2 wt%] to $(Mg_{0.41}Fe_{0.59})O$ [FeO content 56 wt%], at HP/HT conditions, and at the same time to calculate the thermodynamic properties for ferropericlase having $(Mg_{0.54}Fe_{0.46})O$ stoichiometry (Fe_{46} ferropericlase for short) either at ambient condition or at simultaneous HP/HT conditions. The reliability of the QHA at simultaneous HP/HT conditions has been discussed by Scanavino et al. (2012) and in this work QHA is considered reliable as well, in all the P/T ranges treated. Since the maximum iron concentration considered in this work corresponds to the $(Mg_{0.41}Fe_{0.59})O$ stoichiometry, and since the pressure range here investigated corresponds to the one of the lower mantle (from 24 GPa to 136 GPa), we decide to use the LS configuration as such configuration is the most stable at the deeper lower mantle P/T conditions, at least for the iron concentrations considered. A comparison with properties of the HS phase (from literature data) is made as at shallower depth there is a very large region of mixed spin where the properties are intermediate between those of the high-spin and of the low-spin.

This work is the follow-up of a previous one of ours (Scanavino et al. 2012), where we studied the periclase and the LS ferropericlase having a low iron concentration $(Mg_{0.97}Fe_{0.03})O$. In that work we observed how a very low percentage of iron (Fe_{03} ferropericlase) in the structure of periclase significantly changes its static and thermoelastic properties by producing an increase of the bulk modulus both at static (from 163.75 GPa to 172.17 GPa), and at ambient conditions (from 160.14 to 167.42 GPa), and a decrease of the cell volume (from 75.089 $Å^3$ to 74.190 $Å^3$ at static conditions, and

from 75.999 Å^3 to 75.145 Å^3 at ambient conditions). Such trends have also been observed by the computational work of Persson et al. (2006), which reported at static conditions for LS ferropericlase an increase of K_0 (from 153 GPa to 170 GPa) and a decrease of V_0 (from 77.04 Å^3 to 74.96 Å^3).

In view of what is reported above, in this work we set the goal to fill these gaps in the knowledge of LS ferropericlase through the calculation of the P/T dependence of its thermoelastic and thermodynamic properties, for different compositions of $(Mg_{1-x}Fe_x)O$ with x ranging from 0.06 to 0.59.

Computational details

The ground state wave functions, the corresponding energies at the static limit (E_{st}; no inclusion of zero point and thermal energies; see Prencipe et al. (2011) for the definitions), the optimized geometries and the vibrational frequencies are all calculated from first principles, at different cell volumes, by means of the CRYSTAL09 code (Dovesi et al. 2010). For a detailed description of the methodology employed by the code see (Pisani 1996).

To obtain the stoichiometric compositions from $(Mg_{0.94}Fe_{0.06})O$ to $(Mg_{0.41}Fe_{0.59})O$ it is necessary to construct supercells of MgO, and to substitute Fe^{2+} for some of the Mg cations within the structure. As a good compromise between the availability of computational resources and supercell dimensions, calculations are performed on a 2x2x2 supercell (64 atoms in the cell) with respect to the conventional one of periclase (8 atoms). With such a supercell, the different distributions of Fe and Mg in the crystal structure give rise to a generally large number of atomic configurations; precisely the total number p of configurations (if equivalence by symmetry is not taken into account) is equal to $N!/x!(N-x)!$ where N is the number of sites and x the number of substitutions. By considering the symmetry, the whole set of configurations is then arranged in non-equivalent classes, each one being constituted by all the symmetry equivalent configurations. Because the number of such classes is very high [they are a few

hundreds for $(Mg_{0.94}Fe_{0.06})O$, and more than three hundred million for $(Mg_{0.41}Fe_{0.59})O$], for each stoichiometry we chose the ones preserving the highest number of symmetry operators. Such a choice is mainly imposed by the availability of the computational resources; as an example, by considering the $(Mg_{0.94}Fe_{0.06})O$ composition, there are 496 possible configurations which are arranged in 177 classes, and there is only one class that preserves all the 48 symmetry operators. By adding one iron atom more to the previous supercell, the number of classes and configurations increase by about one order of magnitude. Therefore, the calculation of the static energies of the classes preserving the highest symmetry is the unique practical choice.

The chosen basis set of the elements and the thresholds controlling the accuracy of the static energy calculations are specified in (Scanavino et al. 2012). The Hamiltonian chosen (WC1LYP) is a hybrid HF/DFT one, based on the WC (GGA; Generalized Gradient Approximation) exchange functional proposed by Wu and Cohen (Wu and R. Cohen 2006), mixed with 16% of the *exact non-local* Hartree-Fock exchange, and employing the LYP correlation functional proposed by Lee, Yang and Parr (1988). Such percentage of exact Hartree-Fock exchange is essential for the correct reproduction of the elastic and vibrational properties, as demonstrated in previous works that employ this functional (Zicovich-Wilson et al. 2004; Demichelis et al. 2009; Ungureanu, Cossio, and Prencipe 2010; De La Pierre et al. 2011; Prencipe et al. 2012; Prencipe 2012; Scanavino et al. 2012; Ungureanu, Cossio, and Prencipe 2012).

Cell volume (V_0), cell parameter (a_0) and fractional coordinates are optimized by analytical gradient methods, as implemented in CRYSTAL09 (Dovesi et al. 2010). The thresholds controlling the geometry optimizations (TOLDEG and TOLDEX parameters in CRYSTAL09) are respectively 0.0002 hartree/bohr for the components of the gradient and 0.0008 bohr for the displacements.

Normal vibrational modes and their frequencies are calculated for 7 different cell volumes in the [401, 571 $Å^3$] range, for both periclase and Fe_{46} ferropericlase, by diagonalizing a mass-weighted Hessian

matrix (Pascale et al. 2004). The first derivatives of the energy with respect to the atomic positions are calculated analytically (Doll, Saunders, and Harrison 2001), whereas second derivatives are calculated numerically by setting to 0.0015 Å the nuclear displacements with respect to the equilibrium positions. The threshold for the convergence of the total energy, in the self consistent field cycles, is set to 10^{-9} hartree (TOLDEE parameter in CRYSTAL09; (Dovesi et al. 2010).

For each vibrational mode, the mode-γ Grüneisen's parameter (Anderson 1995) is estimated through the analytical derivative of frequency as a function of volume, reconstructed by curve fitting to a quadratic polynomial.

Thermoelastic and thermodynamic properties (total pressure P, static bulk modulus K_0, thermal bulk modulus K_T, thermal expansion α, entropy S and heat capacity C_V and C_P) are obtained in the limit of the QHA, through the evaluation of the dependence of frequencies of the vibrational normal modes by the cell volume (mode-γ Grüneisen's parameters). Intrinsic anharmonic effects (Oganov and Dorogokupets 2004) are not taken into account as in our previous work (Scanavino et al. 2012) we have demonstrated that at simultaneous HP/HT conditions, the Born-Oppenheimer potential energy surface in the neighbourhood of its minimum, corresponding to the stable nuclear configuration, can reasonably be considered harmonic.

The K_0, K', V_0 and a_0 static parameters at the equilibrium are obtained by fitting $E_{st}(V)$ data to a volume integrated third-order Birch-Murnaghan (Birch 1952) equation of state (EoS; BM3, for short, in the following). The same parameters at ambient conditions (P = 0.1 MPa T = 298 K) are obtained by fitting the total $P(V, T)$ curve to BM3 EoS. For some configurations we use also a volume integrated Vinet equation of state (Vinet, Smith, et al. 1987; Vinet, Ferrante, et al. 1987). Other equations of state (Murnaghan, Natural Strain) are not used as not suitable for our wide compression range (Angel 2000).

Results and discussion

188

189 The static energies for each iron composition are calculated at 12 different volumes for different
190 compression ranges according to the composition. The higher is the iron content, the lower is the
191 compression range as, at very compressed volumes and with high concentrations of iron, it is difficult
192 to obtain the SCF convergence. The compression ranges used (expressed as V/V_0) [0.732, 1.028],
193 [0.703, 1.028], [0.657, 1.028], correspond respectively to the pressure ranges [-5, 120/134] GPa, [-5,
194 125/166] GPa and [-5, 177] GPa (the higher is the iron content the higher is the maximum pressure).
195 The resulting EoS parameters for the static fitting are shown in Table 1. Both the EoS's employed
196 (volume integrated BM3 and Vinet) show an increase of the equilibrium bulk modulus with the iron
197 content (Figure 1) and a simultaneous decrease of the equilibrium cell volume (Figure 2), whereas K'
198 shows a non linear increase with the iron content. Although at first sight the differences between the
199 two volume integrated BM3 and Vinet EoS's could appear small, they are not negligible as, for the E_0
200 resulting by the two fitting (not reported in Table 1), the differences are significantly high: about 0.0005
201 hartree for BM3 with respect to static equilibrium E_0 obtained by the geometry optimization, about 5
202 hartree for the Vinet. This demonstrates how the Vinet EoS is not suited for fitting in such pressure
203 ranges.
204 The absence of literature data in Table 1 is due to the lack of computational works concerning
205 ferropericlase at static conditions with the LS configuration, apart from the paper by Persson et al.
206 (2006), whose results are reported in Figure 1 and Figure 2. The deviance of the values obtained in
207 Persson et al. (2006) with respect our data is mainly due to their employed functional as it is known
208 that GGA ones overestimate the cell volume and underestimate the bulk modulus (Alfredsson et al.
209 2005). Apart from this their trends fully confirm our data. Experimental papers are obviously absent
210 because of the impossibility to reach static conditions experimentally. In Table 2 are reported the cell
211 volumes for the LS phase obtained by geometry optimization: the difference with the data obtained by

EoS fitting is minimal (about 2 mHa). Experimental data are again absent due to the impossibility to obtain a crystal of LS ferropericlase at ambient conditions.

Starting from the calculated frequencies of the vibrational modes it is possible to obtain the vibrational energies, which provide the equilibrium thermodynamic parameters at ambient condition of periclase and Fe_{46} ferropericlase (Table 3). By looking at our data in Table 3, it is possible to confirm what was already observed in our previous work (Scanavino et al. 2012): a reduction of the pressure range in the fitting reduces K_0 and increases V_0. Moreover, as already noted for the static fitting, the Vinet EoS overestimates the cell volume and underestimates the bulk modulus. A comparison with other literature data reported in Table 3 is difficult since the fittings by Lin et al. (2005) and Fei et al. (2007) are made by using a second order Birch-Murnaghan EoS (BM2), which is not suitable in this range of pressure, according to Angel (2000) and Scanavino et al. (2012). Such inadequacy is also confirmed by the fact that starting from the data of Lin et al. (2005) and fitting them by using a BM3 EoS, we obtain very different results (Table 3), with respect to those reported by Lin et al. (2005) themselves.

The only comparable datum for the LS ferropericlase is the one by Speziale et al. (2007), who for a $(Mg_{0.83}Fe_{0.17})O$ stoichiometry, observed a reduction of the cell volume and an increase of the bulk modulus, consistently with what is observed in the present work. The comparison with the HS phase is relatively easier due to the greater number of works dealing with this phase [(Bonzcar and Graham 1982; Jacobsen et al. 2002; Kung et al. 2002; Lin et al. 2005; Jackson et al. 2006; Speziale et al. 2007; Fei et al. 2007; Reichmann et al. 2008; Komabayashi et al. 2010; Matsui et al. 2012) - see Table 4]. In contrast with the LS phase, in the HS it is possible to observe that K_0 is almost unmodified by the increase of iron; but V_0 increases with the iron content and, in this respect, shows an opposite behaviour with respect to the LS phase.

The reliability of our fittings, both at static and at ambient conditions, is confirmed by the F-f plots (Angel 2000) showing that Fe_{46} ferropericlase is correctly described by the BM3 EoS (Figure 3).

As regards the mode-γ Grüneisen's parameter, the average value related to vibrational modes at the static equilibrium volume for Fe_{46} ferropericlase increases with respect to those for periclase [from 1.112 for periclase to 1.257 for $(Mg_{0.97}Fe_{0.03})$ (Scanavino et al. 2012), and to 1.291 for Fe_{46} ferropericlase], due to the reduction of the values of the frequencies and of the relative cell volume at the static equilibrium.

Some thermoelastic (K_T, V_T, K'_T, α) and thermodynamic parameters of interest (C_V, C_P, S) are shown in Table 5, concerning either periclase (Isaak, Anderson, and Goto 1989; Chopelas 1990; Fei 1995; Inbar and R.E. Cohen 1995; Robie, Hemingway, and Fisher 1995; Dubrovinsky and Saxena 1997; Fiquet, Richet, and Lyon 1999; Karki et al. 2000; Oganov and Dorogokupets 2003; Oganov, Gillan, and Price 2003; Ghose et al. 2006) or LS and HS-ferropericlase [however, in some works the spin is not specified (Hama and Suito 1999)] with different iron contents (the thermoelastic ones are calculated numerically).

As regards the LS phase, the thermal expansion shows significant variation as it decreases from $2.25*10^{-5}$ K^{-1} for periclase, to $1.97*10^{-5}$ K^{-1} for Fe_{46} ferropericlase, but such a decrease is not linear as the value of α for the Fe_{03} ferropericlase is $2.43*10^{-5}$ K^{-1}, that is, it is a higher value than the corresponding one for periclase. Such trend of the thermal expansion as a function of composition can also directly be seen in the increase of the cell volume in the passage from static to ambient conditions. In fact, when we calculate the cell volume at ambient condition, we have to consider both the zero point and thermal effects of the vibrational normal modes of the crystal. Both effects generate an additional pressure that sums to the static one (the *zero-point* pressure and the thermal pressure). It means that at 300 K, but also at every other temperature (0 K included), these pressures are to be taken into account whereas, by definition, they are absent at the static condition. In particular, such pressures must be compensated by the static one in order to keep the crystal at the equilibrium with the imposed external pressure (Prencipe et al. 2011). As *zero-point* and thermal pressure are generally positive,

static pressure must assume negative values corresponding to larger cell volumes with respect to the static one. By excluding the *zero-point* pressure (+1.23 GPa for periclase and +1.71 GPa for Fe_{46} ferropericlase), as it is not dependent by the temperature, and with respect to the cases at 0K, at 300K we calculate a volume expansion of +0.91 $Å^3$ for periclase and +0.79 $Å^3$ for ferropericlase due to a corresponding increase of the thermal pressure from 0 to about +0.54 GPa for both compositions.

Such reduction of the thermal expansion is in contrast to the findings of Zhang and Kostak (1992), who observed that the thermal expansion and the thermodynamic parameters are not influenced by the iron content. Such a statement, that is not valid for the LS phase, is consistent with the data for the HS phase (Fei et al. 1992; J. Zhang and Kostak 2002), which are indeed not significantly dependent upon the iron concentration.

The other thermodynamic quantities of Table 5 appear to remain almost unmodified by the presence of iron, except for C_P obtained for $(Mg_{0.60}Fe_{0.40})O$ by Fei et al. (1999) and Zhang and Kostak (2002), which respectively obtained a lower and a higher value with respect to the one of periclase, although they treated a high-spin ferropericlase.

As regards the thermoelastic quantities, they agree with the same quantities obtained by a EoS fitting reported in Table 3 (the maximum differences are -0.034 $Å^3$ for the volume of Fe_{46} ferropericlase and +1.35 GPa for the bulk modulus of Fe_{03} ferropericlase).

Lastly we calculate for Fe_{46} ferropericlase the values of the thermal expansion coefficient α (Figure 4), of the K_0 (Figure 5), of the heat capacity C_V and C_P (Figure 6) and of the entropy S (Figure 7) as a function of the depth, or according to the conditions of pressure and temperature of the geobar curve (Bina 1998) and of the geotherm curve (Brown and Shankland 1981) respectively. As regards the thermal expansion, we notice that Fe_{46} ferropericlase has lower values with respect to periclase in all the lower mantle and ambient conditions, whereas the bulk modulus of Fe_{46} ferropericlase is always larger. The values of the heat capacity and of the entropy appear to be almost constant in the lower

mantle. We recall that the LS phase, with the $(Mg_{0.54}Fe_{0.46})O$ stoichiometric composition, becomes the most stable one at about 60 GPa, corresponding to about 1500 km of depth; this does not mean that the results for shallower depths are meaningless or wrong: the curves reported in Figures 4, 5, 6 and 7 do describe the correct behavior of the low-spin phase for those P/T conditions, even if such phase is not the most stable one. Moreover the expected FeO content of ferropericlase in the lower mantle ranges from 15 to 20 mole% (Fei et al. 2007), and at such composition the low spin phase becomes the most stable even at shallower depths.

Finally, the data proposed in this work could be used for the calculation of the longitudinal seismic velocities. Since the speed of the longitudinal waves is proportional to the bulk modulus, one could say that we expect an increase in the velocity of seismic waves with respect to the case of periclase, but such prediction is strictly conditioned by the value of the density, that with the *ab-initio* techniques can not be determined in precise way. Consequently the only reliable data concern the bulk modulus and its P/T/X dependence and these data can subsequently be entered in the geodynamic models integrated with other data from another source (density, shear modulus,...) to obtain the change in the seismic speeds.

Tables and Figures

Table 1 - Equilibrium values of K_0 , K' and V_0 at static condition for the low-spin (LS) ferropericlase sorted according to the percentage of iron. The iron percentage is referred to the stoichiometric formula $(Fe_{\delta/100}Mg_{1-(\delta/100)})O$. The letters a, b, c and d, used in the column of the iron percentage, indicate different configurations ordered as a function of decreasing static energy. The compression ranges are referred to the ratio V/V_0.

	[0.657, 1.028] compression range						**[0.703, 1.028] compression range**						**[0.732, 1.028] compression range**		
	BM3			**Vinet**			**BM3**			**Vinet**			**BM3**		
% Fe [δ]	**K_0 [GPa]**	**K'**	**V_0 [Å^3]**	**K_0 [GPa]**	**K'**	**V_0 [Å^3]**	**K_0 [GPa]**	**K'**	**V_0 [Å^3]**	**K_0 [GPa]**	**K'**	**V_0 [Å^3]**	**K_0 [GPa]**	**K'**	**V_0 [Å^3]**
3*	172.17	4.10	74.190												
6a	175.09	4.097	73.870				174.41	4.118	73.884						
6b	175.53	4.086	73.859	169.91	4.458	73.938	174.75	4.109	73.876						
6c	175.11	4.090	73.868				174.35	4.113	73.883						
9a	179.62	4.054	73.535	174.63	4.403	73.591	178.06	4.103	73.562						
9b	179.62	4.054	73.535				178.06	4.103	73.562						
12a	183.83	4.015	73.200	178.90	4.351	73.254	181.19	4.097	73.245						
12b	182.37	4.092	73.352				180.79	4.142	73.379						
12c	182.37	4.092	73.352				180.79	4.142	73.379						
12d	183.83	4.015	73.200				181.19	4.097	73.245						
15a	186.29	4.053	73.010	181.07	4.402	73.066	183.87	4.126	73.050						
15b	186.29	4.126	73.010				183.87	4.053	73.050						
18	189.18	4.074	72.807	183.84	4.432	72.872	186.55	4.151	72.853						
21a	188.64	4.142	72.967	178.88	4.535	72.841	184.76	4.150	72.772						
21b	188.64	4.142	72.967				185.32	4.240	73.026						
25							188.90	4.210	72.783	184.82	4.535	72.818			
37a							200.73	4.287	72.058	195.89	4.636	72.101	199.69	4.322	72.072
37b							200.73	4.287	72.058				199.69	4.322	72.072
40a							204.76	4.223	71.890				203.12	4.277	71.912
40b							204.73	4.267	71.777	199.83	4.612	71.821	203.35	4.312	71.796
40c							204.78	4.222	71.892	200.07	4.556	71.933	203.11	4.276	71.915
46a							210.75	4.283	71.423	205.67	4.631	71.466	209.43	4.325	71.440
46b							210.59	4.274	71.574				209.13	4.321	71.969
46c							210.74	4.283	71.548				209.43	4.325	71.941
56							220.49	4.256	71.030	215.27	4.598	71.072	218.45	4.318	71.055
59							224.92	4.204	70.809	219.77	4.535	70.850	222.26	4.283	70.842

* The datum is from Scanavino et al. (2012).

313

Table 2 - Equilibrium values of cell volume at static condition for the low-spin (LS) ferropericlase sorted according to the percentage of iron. The iron percentage is referred to the stoichiometric formula ($Fe_{\delta/100}Mg_{1-(\delta/100)}$)O. The letters a, b, c and d, used in the column of the iron percentage, indicate different configurations ordered as a function of decreasing static energy. The data are otained by geometry optimization.

	Fe % [δ]	Volume [Å^3]		Fe % [δ]	Volume [Å^3]		Fe % [δ]	Volume [Å^3]
Scanavino et al. (2012)	3	74.121	This work	15a	73.414	This work	40c	71.908
This work	6a	73.813	This work	15b	73.414	This work	46a	71.572
This work	6b	73.815	This work	18	73.210	This work	46b	71.555
This work	6c	73.807	This work	21a	72.961	This work	46c	71.395
This work	9a	73.963	This work	21b	72.961	This work	56	71.020
This work	9b	73.963	This work	25	72.738	This work	59	70.810
This work	12a	73.632	This work	37a	72.007			
This work	12b	73.744	This work	37b	72.008			
This work	12c	73.744	This work	40a	71.916			
This work	12d	73.632	This work	40b	71.666			

314

Table 3 - Equilibrium values of K_0, K' and V_0 at ambient condition for the low-spin (LS) ferropericlase sorted according to the percentage of iron. The iron percentage is referred to the stoichiometric formula ($Fe_{\delta/100}Mg_{1-(\delta/100)}$)O.

	P(V) fitting interval [GPa]	% Fe [δ]	EoS	K_0 [GPa]	K'	V_0 [Å^3]	Methodology
Scanavino et al. (2012)	0 - 170	3	BM3	167.42	4.09	75.145	HF/DFT (WC1LYP)
Lin et al. (2005)	55 - 135	17	BM2	250	4 (fixed)	/	X-ray diffraction
Lin et al. (2005)	55 - 135	17	Vinet	245	4 (fixed)	/	X-ray diffraction
Scanavino et al. (2012)	80 - 135	17	BM3	164.57[§]	4.61[§]	71.551[§]	
Speziale et al. (2007)	80 - 135	17/20	BM3	190[§]	4.60[§]	71.000[§]	
Speziale et al. (2007)	40 - 134	17	BM3	186	4.60	71.390	X-ray diffraction
Fei et al. (2007)	40 - 95	20	BM2	170	4 (fixed)	74.200	X-ray diffraction
Mao et al. (2012)	0 - 140	25	BM2	166	4 (fixed)	74.4	X-ray diffraction
Fei et al. (2007)	60 - 148	39	BM2	170	4 (fixed)	73.600	X-ray diffraction
This work	0 – 158.62	46	BM3	205.57	4.242	72.216	HF/DFT (WC1LYP)
	0 – 158.62	46	BM4	206.05	4.207	72.173	HF/DFT (WC1LYP)
	0 – 158.62	46	Vinet	198.22	4.642	72.319	HF/DFT (WC1LYP)
	0 – 128.73	46	BM3	204.13	4.279	72.244	HF/DFT (WC1LYP)
	0 – 128.73	46	BM4	205.82	4.206	72.182	HF/DFT (WC1LYP)
	0 – 128.73	46	Vinet	198.45	4.635	72.315	HF/DFT (WC1LYP)

The symbol / means that the datum is not reported.
[§] the fitted data are from Lin et al. (2005)

315

Table 4 - Equilibrium values of K_0, K' and V_0 at static and at ambient conditions for the high-spin (HS) ferropericlase sorted according to the percentage of iron. The iron percentage is referred to the stoichiometric formula $(Fe_{\delta/100}Mg_{1-(\delta/100)})O$.

	***P(V)* fitting interval [GPa]**	**% Fe [δ]**	**EoS**	**K_0 [GPa]**	**K'**	**V_0 [Å^3]**	**Methodology**
Static conditions							
Scanavino et al. (2012)	0 -180	3	BM3	175.87	4.243	73.789	HF/DFT (HF 35%)
Scanavino et al. (2012)	0 -180	3	BM3	168.93	/	74.739	HF/DFT (WC1LYP)
Persson et al. (2006)	-20 - 200	25	BM3	153	4.1	79.120	GGA + PAW
Persson et al. (2006)	-20 - 200	50	BM3	163	4.0	80.600	GGA + PAW
Persson et al. (2006)	-20 - 200	75	BM3	148	4.4	82.800	GGA + PAW
Ambient conditions							
Reichmann et al. (2008) *	0 - 9	1.3	#	161.1	4.2	/	Brillouin spectroscopy
Jackson et al. (2006)	0 - 20	6	#	163	3.90	/	Brillouin spectroscopy
Jacobsen et al. (2002)	/	6	/	161°	/	75.098	X-ray diffraction
Bonzcar and Graham (1982)	0 – 0.5	8	d	159.5	3.66	75.312	X-ray diffraction
Jacobsen et al. (2002)	/	15	/	166°	/	75.633	X-ray diffraction
Kung et al. (2002) *	0 - 10	17	#	165.6	4.14	75.848	X-ray diffraction
Lin et al. (2005)	0 - 55	17	BM3	160.7	3.280	/	X-ray diffraction
Lin et al. (2005)	0 - 55	17	Vinet	161.3	3.25	/	X-ray diffraction
Matsui et al. (2012)	0 - 53	17	BM3	160 (fixed)	4.08	75.849	X-ray diffraction
Scanavino et al. (2012)	0 - 53	17	BM3	175.58[a]	3.11[a]	76.179[a]	
Speziale et al. (2007)	0 - 40	17/20	BM3	157.5[b]	3.92[b]	76.10[b]	X-ray diffraction
Wu et al. (2009)	0 - 150	18.75	/	172.48	/	76.16	LDA+U
Komabayashi et al. (2010)	15 - 72	19	BM2	154.3	4 (fixed)	76.24	X-ray diffraction
Speziale et al. (2007)	0 - 40	20	BM3	158	4.4	76.030	X-ray diffraction
Scanavino et al. (2012)	0 - 40	20	BM3	154.42[c]	3.91[c]	76.140[c]	
Fei et al. (2007)	0 - 35	20	BM2	158	4 (fixed)	76.16	X-ray diffraction
Jacobsen et al. (2002)	/	24	/	165°	/	76.333	X-ray diffraction
Mao et al. (2012)	0 - 140	25	BM2	162	4 (fixed)	76.34	X-ray diffraction
Matsui et al. (2012)	0 - 55	25	BM3	160 (fixed)	4.22	76.372	X-ray diffraction
Jacobsen et al. (2002)	0 – 9.3	27	BM3	158.4	5.49	76.336	X-ray diffraction
Scanavino et al. (2012)	0 – 9.3	27	BM3	158.32[g]	5.42[g]	76.336[g]	
Bonzcar and Graham (1982)	0 – 0.5	27.5	d	167.6	3.93	76.187	X-ray diffraction
van Westrenen et al. (2005) *	0 – 26.7	36	BM3	154	4	77.438	X-ray diffraction

Jacobsen et al. (2002)	/	37	/	164	/	76.836	X-ray diffraction
Fei et al. (2007)	0 - 60	39	BM2	156	4 (fixed)	77.480	X-ray diffraction
Fei et al. (1992) *	8 - 30	40	BM2	157	4 (fixed)	77.417	X-ray diffraction
Zhang and Kostak (2002) *	0 – 10.1	40	BM2	158	4 (fixed)	77.460	X-ray diffraction
Bonzcar and Graham (1982)	0 – 0.5	40.5	d	161.5	6.18	77.064	X-ray diffraction
Bonzcar and Graham (1982)	0 – 0.5	41.6	d	168.7	/	76.766	X-ray diffraction
Jacobsen et al. (2002)	/	53	/	161	/	77.937	X-ray diffraction
Jacobsen et al. (2002)	0 – 8.9	56	BM3	155.8	5.53	77.453	X-ray diffraction
Fei et al. (2007)	0 - 42	59	BM2	153	4 (fixed)	79.360	X-ray diffraction

The symbol / means that the datum is not reported
° adiabatic K_0 obtained from elastic constants
Finite- strain equation of state taken from Davies and Dziewonski (1975)
d From elastic constant
[a] the fitted data are from Matsui et al. (2012)
[b] combined dataset from Lin et al. (2005) and Speziale et al. (2005)
[c] the fitted data are from Speziale et al. (2007)
[g] the fitted data are from Jacobsen et al. (2002)
* the spin state of the iron is not specified

316

317

318

319

320

321

322

323

324

325

326

327

328

329

330

Table 5 – Comparison of some thermoelastic (V_T, K_T, K'_T, α) and thermodynamic parameters of interest (C_V, C_P, S) for periclase and ferropericlase. The molar quantities are converted for the primitive cell of periclase with two atoms in order to allow the comparison, whereas the cell volume refers to the conventional cell with eight atoms [P = 0.1 MPa , T = 298.15 K].

	V_T [Å^3]	K_T [GPa]	K'_T	C_V [J/(mole* K)]	C_P [J/(mole* K)]	S [J/(mole* K)]	α [1/K]	Spin state
MgO								
Inbar and Cohen (1995)	/	/	/	/	/	/	3.88E-05	
Ghose et al. (2006)	/	/	/	36.58	/	26.80	/	
Fiquet et al. (1996)	/	/	/	/	/	/	4.90E-05	
Fiquet et al. (1999)	74.725	/	/	36.20	/	/	3.19E-05	
Dubrovinsky and Saxena (1997)	/	/	/	/	/	/	3.15E-05	
Saxena et al. (1993)	/	/	/	36.82	37.35	26.94	3.12E-05	
Fei (1995)	/	/	/	/	/	/	3.16E-05	
Chopelas (1990)	/	/	/	36.74	/	26.84	3.11E-05	
Isaak et al. (1989)	/	/	/	/	37.67	/	3.12E-05	
Robie and Hemingway (1995)	/	/	/	36.87	/	/	/	
Scanavino et al. (2012) #	75.999	162.19	4.204	35.474	35.755	25.133	2.25E-05	
Hama and Suito (1999) #	74.724	160.2	4.52	36.5	/	26.6	/	
Oganov and Dorogokupets (2003) #	74.670	170.53	4.036	/	31.3	/	2.40E-05	
Oganov et al. (2003) #	76.225	172.6	4.004	/	/	26.81	/	
Karki et al. (2000) #	74.240	159	4.30	36.53	37.06	26.65	3.11E-05	
$Mg_{0.97}Fe_{0.03}O$								
This work #	75.144	168.77	4.056	35.46	35.80	25.04	2.43E-05	LS
Hama and Suito (1999) #	73.594*	160.16[§]	4.638[§]	/	/	/	/	/
$Mg_{0.8125}Fe_{0.1875}O$								
Wu et al. (2009)	76.16	172.48	/	38.98	39.66	/	3.35E-05	HS
$Mg_{0.75}Fe_{0.25}O$								
Mao et al. (2011)	76.34	162	/	/	/	/	3.76E-05	HS
Mao et al. (2011)	74.4	166	/	/	/	/	3.37E-05	LS
$Mg_{0.60}Fe_{0.40}O$								
Fei et al. (1992)	77.418	157	/	/	27.54	/	3.95E-05	HS
Zhang and Kostak (2002)	77.460	158	/	41.12	41.92	/	3.79E-05	HS
$Mg_{0.54}Fe_{0.46}O$								
This work #	72.182	206.27	4.187	36.11	36.38	26.62	1.97E-05	LS
Hama and Suito (1999) #	76.323*	167.60*	3.790*	/	/	/	/	/

The symbol / means that the datum is not reported
computational works [HF/DFT this work; LDA Karki et al. (2000), Oganov et al. (2003); GGA Oganov and Dorogokupets (2003), thermodinamic model Hama and Suito (1999)]
[§] the data are obtained by relations of the type $V_T(MgFeO)=V_T(MgO)[1+a_1 y+ a_2 y^2 + a_3 y^3]$ where y is the iron content in the stoichiometric formula $Mg_{1-y}Fe_yO$

331

332

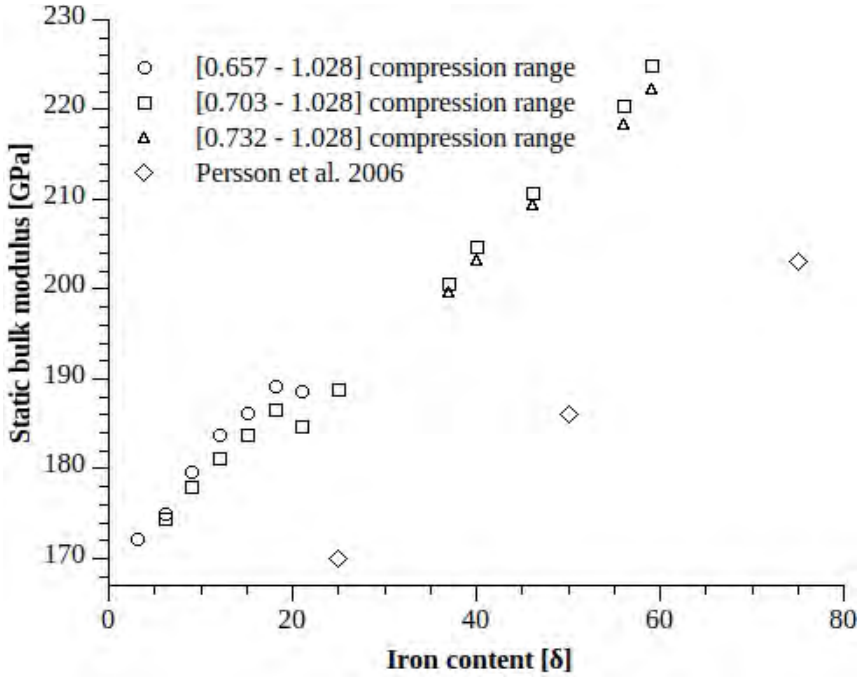

Figure 1

333

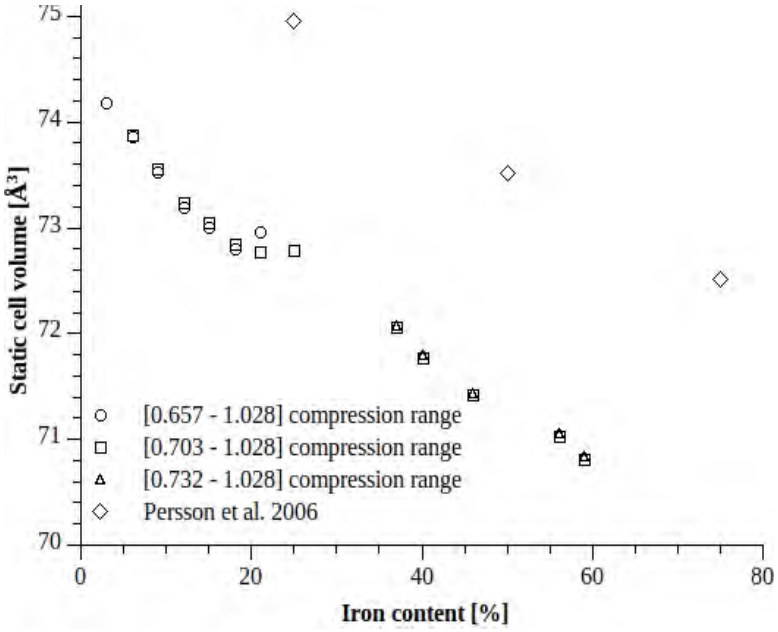

Figure 2

334

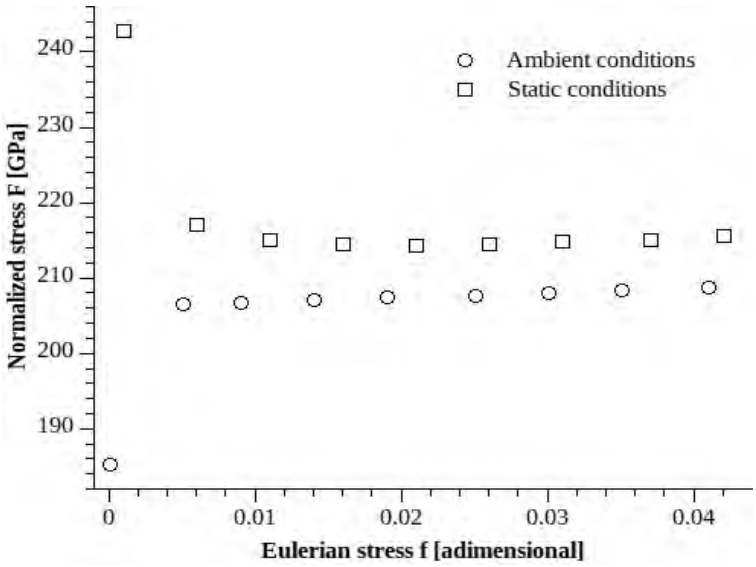

Figure 3

335

336

337

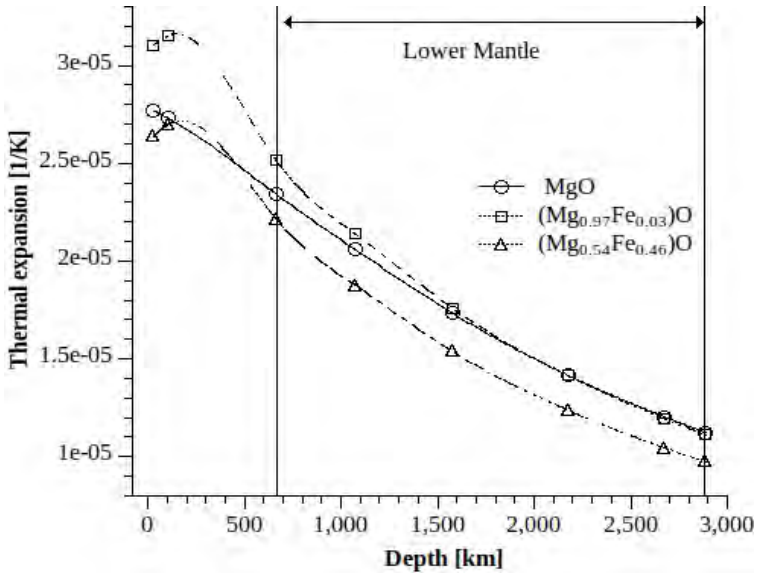

Figure 4

338

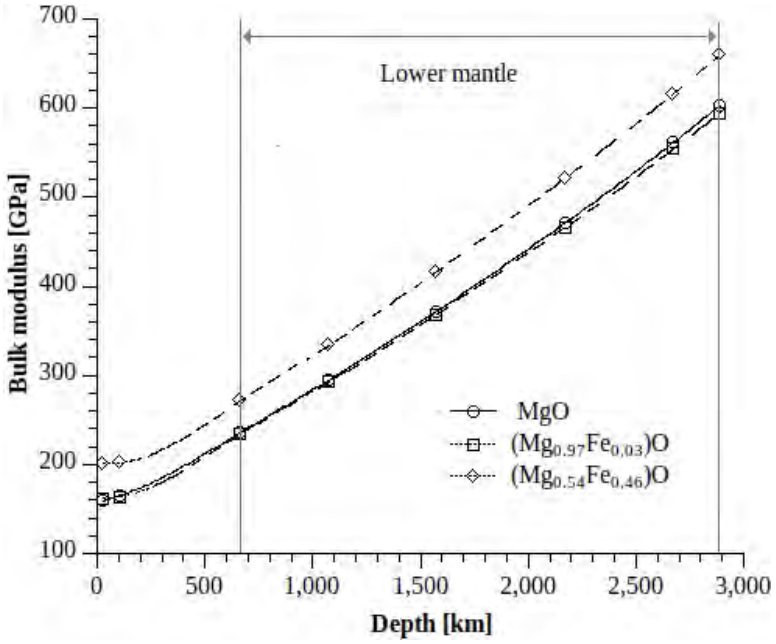

Figure 5

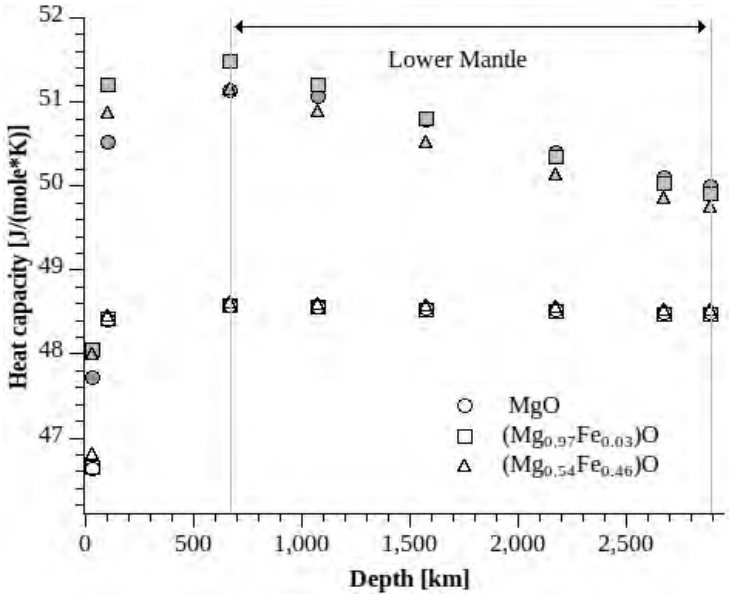

Figure 6

339

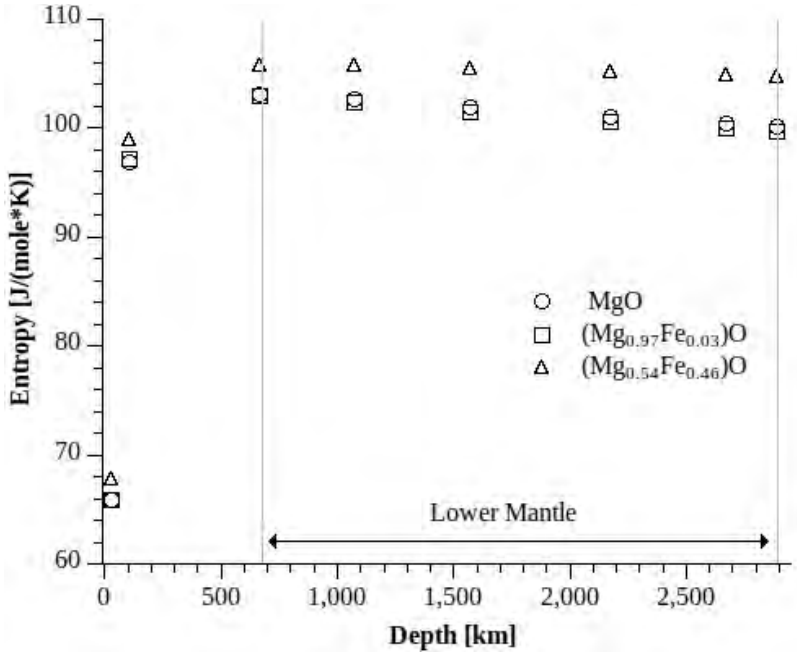

Figure 7

340

341

342

343

344

345

346

347

348

349

350

351

List of Figures

- Figure 1 - Static bulk modulus of ferropericlase as a function of the iron content in the stoichiometric formula $(Fe_{\delta/100}Mg_{1-(\delta/100)})O$. The datum of Persson et al. 2006 is obtained with a compression range of [-20, 200] GPa.
- Figure 2 - Static conventional cell volume (1/8 of the supercell) of ferropericlase as a function of the iron content in the stoichiometric formula $(Fe_{\delta/100}Mg_{1-(\delta/100)})O$. The datum of Persson et al. 2006 is obtained with a compression range of [-20, 200] GPa.
- Figure 3 - Normalized stress F as a function of Eulerian strain f for ferropericlase $(Mg_{0.56}Fe_{0.46})O$ at static and at ambient conditions.
- Figure 4 - Thermal expansion coefficient as a function depth. The P/T conditions reflect the ones of the Earth's interior according the values of the geotherm and the geobar curves. At the points indicated in the figure correspond the following P/T conditions: 25 km (0.6 GPa / 773 K); 100 km (3.3 GPa / 1475 K); 660 km (23.5 GPa / 1866 K); 1071 km (41.5 GPa / 2004 K); 1571 km (65.1 GPa / 2147 K); 2171 km (95.3 GPa 2296 K); 2671 km (122.4 GPa / 2405 K); 2885 km (134.8 GPa / 2449 K).
- Figure 5 - Bulk modulus as a function of depth. The P/T conditions reflect the ones of the Earth's interior according the values of the geotherm and the geobar curves. For the P/T conditions associated at the points in the picture see the caption of Figure 4.
- Figure 6 - Heat capacity as a function of depth. The P/T conditions reflect the ones of the Earth's interior according the values of the geotherm and the geobar curves. For the P/T conditions associated at the points in the picture see the caption of Figure 4. The empty symbols refer to the C_V, the full ones to the C_P.

- Figure 7 - Entropy as a function of depth. The P/T conditions reflect the ones of the Earth's interior according the values of the geotherm and the geobar curves. For the P/T conditions associated at the points in the picture see the caption of Figure 4.

References

Alfredsson, M., Brodholt, J.P., Wilson, P.B., Price, G.D., Corà, F., Calleja, M., Bruin, R., Blanshard, L.J., and Tyer, R.P. (2005) Structural and magnetic phase transitions in simple oxides using hybrid functionals. Molecular Simulation, 31, 367–377.

Anderson, O.L. (1995) Equations of state of solids for geophysics and ceramic science, Oxford University Press, New York.

Angel, R.J. (2000) Equation of State. Reviews in Mineralogy and Geochemistry, 41, 35–59.

Badro, J., Struzhkin, V.V., Shu, J., Hemley, R.J., Mao, H. (1999) Magnetism in FeO at Megabar Pressures from X-Ray Emission Spectroscopy. Physical Review Letters, 83, 4101-4104.

Bina, C.R. (1998) Lower mantle mineralogy and the geophysical perspective. In R.J. Hemley, Ed., Ultrahigh-pressure mineralogy: Physics and chemistry of the earth's deep interior, p. 671. Mineralogical Society of America, Washington.

Birch, F. (1952) Elasticity and constitution of the Earth's interior. Journal of Geophysical Research, 57, 227–286.

Bonzcar, L.J., and Graham, E.K. (1982) The pressure and temperature dependence of the elastic properties of polycrystal magnesiowustite. Journal of Geophysical Research, 87, 1061–1078.

Brown, J.M., and Shankland, T.J. (1981) Thermodynamic parameters in the Earth as determined from seismic profiles. Geophysical Journal International, 66, 579–596.

Chen, B., Jackson, J.M., Sturhahn, W., Zhang, D., Zhao, J., Wicks, J.K., and Murphy, C.A. (2012) Spin

crossover equation of state and sound velocities of $(Mg_{0.65}Fe_{0.35})O$ ferropericlase at 140 Gpa. Journal of Geophysical Research: Solid Earth, 117, B8.

Chopelas, A. (1990) Thermal expansion, heat capacity and entropy of MgO at mantle pressures. Physics and Chemistry of Minerals, 17, 142–148.

Crowhurst, J.C., Brown, J.M., Goncharov, A.F., and Jacobsen, S.D. (2008) Elasticity of (Mg,Fe)O through the spin transition of iron in the lower mantle. Science, 319, 451–453.

Demichelis, R., Civalleri, B., Ferrabone, M., and Dovesi, R. (2009) On the Performance of Eleven DFT Functionals in the Description of the Vibrational Properties of Aluminosilicates. International Journal, 110, 406–415.

Doll, K., Saunders, V.R., and Harrison, N.M. (2001) Analytical Hartree–Fock gradients for periodic systems. International Journal of Quantum Chemistry, 82, 1–13.

Dovesi, R. et al. (2010) CRYSTAL09 user's manual.

Dubrovinsky, L.S., and Saxena, S.K. (1997) Thermal Expansion of Periclase (MgO) and Tungsten (W) to Melting Temperatures. Physics and Chemistry of Minerals, 8, 547–550.

Fei, Y. (1995) Thermal Expansion. AGU Reference Shelf.

Fei, Y. (1999) Effects of temperature and composition on the bulk modulus of (Mg,Fe)O. American Mineralogist, 84, 272–276.

Fei, Y., Mao, H., Shu, J., and Hu, J. (1992) P-V-T equation of state of Magnesiowustite $(Mg_{0.6}Fe_{0.4})O$. Physics and Chemistry of Minerals, 18, 416–422.

Fei, Y., Zhang, L., Corgne, A., Watson, H., Ricolleau, A., Meng, Y., and Prakapenka, V. (2007) Spin transition and equations of state of (Mg,Fe)O solid solutions. Geophysical Research Letters, 34,

L17307.

Fiquet, G., Richet, P., and Lyon, A.D. (1999) High-temperature thermal expansion of lime , periclase , corundum and spinel. Physics and Chemistry of Minerals, 2, 103–111.

Ghose, S. et al. (2006) Lattice Dynamics of MgO at High Pressure: Theory and Experiment. Physical Review Letters, 96, 25–28.

Hama, J., and Suito, K. (1999) Thermoelastic properties of periclase and magnesiowustite under high pressure and high temperature. Physics of the Earth and Planetary Interiors, 114, 165–179.

Inbar, I., and Cohen, R.E. (1995) High Pressure Effects on Thermal Properties of MgO. Geophysical Research Letters, 22, 1533–1536.

Irifune, T. (1994) Absence of an aluminous phase in the upper part of the Earth's lower mantle. Nature, 370, 131–133.

Isaak, D.G., Anderson, O.L., and Goto, T. (1989) Measured elastic moduli of single-crystal MgO up to 1800 K. Physics and Chemistry of Minerals, 16, 704–713.

Jackson, J.M., Sinogeikin, S.V., Jacobsen, S.D., Reichmann, H.J., Mackwell, S.J., and Bass, J.D. (2006) Single-crystal elasticity and sound velocities of $(Mg_{0.94}Fe_{0.06})O$ ferropericlase to 20 GPa. Journal of Geophysical Research, 111, 1–8.

Jacobsen, S.D., Reichmann, H.J., Spetzler, H.A., Mackwell, S.J., Smyth, J.R., Angel, R.J., and Mccammon, C.A. (2002) Structure and elasticity of single-crystal (Mg,Fe)O and a new method of generating shear waves for gigahertz ultrasonic interferometry. Journal of Geophysical Research, 107, 14.

Kantor, I., Dubrovinsky, L., McCammon, C., Steinle-Neumann, G., Kantor, A., Skorodumova, N., Pascarelli, S., Aquilanti, G. (2009) Short-range order and Fe clustering in $Mg_{1-x}Fe_xO$ under high

pressure. Physical Review B, 80, 014204.

Karki, B.B., Wentzcovitch, R.M., Gironcoli, S., and Baroni, S. (2000) High-pressure lattice dynamics and thermoelasticity of MgO. Physical Review B, 61, 8793–8800.

Komabayashi, T., Hirose, K., Nagaya, Y., Sugimura, E., and Ohishi, Y. (2010) High-temperature compression of ferropericlase and the effect of temperature on iron spin transition. Earth and Planetary Science Letters, 297, 691–699.

Kung, J., Li, B., Weidner, D.J., Zhang, J., and Liebermann, R.C. (2002) Elasticity of $(Mg_{0.83},Fe_{0.17})O$ ferropericlase at high pressure□: ultrasonic measurements in conjunction with X-radiation techniques. Earth and Planetary Science Letters, 203, 557–566.

De La Pierre, M., Orlando, R., Maschio, L., Doll, K., Ugliengo, P., and Dovesi, R. (2011) Performance of six functionals (LDA, PBE, PBESOL, B3LYP, PBE0, and WC1LYP) in the simulation of vibrational and dielectric properties of crystalline compounds. The case of forsterite Mg_2SiO_4. Journal of Computational Chemistry, 32, 1775–1784.

Lee, C., Yang, W., and Parr, R.G. (1988) Development of the Colle-Salvetti correlation-energy formula into a functional of the electron density. Physical Review B, 37, 785–789.

Lin, J.F., Heinz, D.L., Mao, H., Hemley, R.J., Devine, J.M., Li, J., and Shen, G. (2003) Stability of magnesiowustite in Earth's lower mantle. Proceedings of the National Academy of Sciences of the United States of America, 100, 4405–4408.

Lin, J.F. et al. (2005) Spin transition of iron in magnesiowustite in the Earth's lower mantle. Nature, 436, 377–380.

Lin, J.F. et al. (2006) Pressure-induced electronic spin transition of iron in magnesiowustite-(Mg,Fe)O. Physical Review B, 73, 73–76.

Lin, J.F. et al. (2007) Spin transition zone in Earth's lower mantle. Science, 317, 1740–1743.

Lin, J.F. And Tsuchiya, T. (2008) Spin transition of iron in the Earth's lower mantle. Physics of the Earth and Planetary Interiors, 170, 248-259.

Mao, H.K., Shen, G., and Hemley, R.J. (1997) Multivariable dependence of Fe-Mg partitioning in the lower mantle. Science, 278, 2098–2100.

Mao, Z., Lin, J., Liu, J., and Prakapenka, V.B. (2011) Thermal equation of state of lower-mantle ferropericlase across the spin crossover. Geophysical Research Letters, 38, L23308

Matsui, M. et al. (2012) Static compression of $(Mg_{0.83},Fe_{0.17})$ and $(Mg_{0.75},Fe_{0.25})$ ferropericlase up to 58 GPa at 300, 700, and 1100 K. American Mineralogist, 97, 176–183.

Oganov, A.R., Brodholt, J.P., and Price, G.D. (2002) Ab initio theory of phase transitions and thermoelasticity of minerals. In C.M. Gramaccioli, Ed., Energy Modelling in Minerals, pp. 83–170, vol. 4. EMU Notes in Mineralogy, Milan.

Oganov, A.R., and Dorogokupets, P.I. (2003) All-electron and pseudopotential study of MgO: Equation of state, anharmonicity, and stability. Physical Review B, 67, 1–11.

Oganov, A.R., and Dorogokupets, P.I. (2004) Intrinsic anharmonicity in equations of state and thermodynamics of solids. Journal of Physics: Condensed Matter, 16, 1351–1360.

Oganov, A.R., Gillan, M.J., and Price, G.D. (2003) Ab initio lattice dynamics and structural stability of MgO. The Journal of Chemical Physics, 118, 10174.

Ottonello, G., Civalleri, B., Ganguly, J., Perger, W.F., Belmonte, D., and Vetuschi Zuccolini, M. (2010) Thermo-chemical and thermo-physical properties of the high-pressure phase anhydrous B $(Mg_{14}Si_5O_{24})$: An ab-initio all-electron investigation. American Mineralogist, 95, 563–573.

Pascale, F., Zicovich-Wilson, C.M., Lopez Gejo, F., Civalleri, B., Orlando, R., and Dovesi, R. (2004) The calculation of the vibrational frequencies of crystalline compounds and its implementation in the CRYSTAL code. Journal of Computational Chemistry, 25, 888–897.

Pasternak, M.P., Taylor, R.D., Jeanloz, R., Li, X., Nguyen, J.H., McCammon, C.A. (1997) High Pressure Collapse of Magnetism in $Fe_{0.94}O$ Mössbauer Spectroscopy Beyond 100 GPa. Physical Review Letters, 79, 5046.

Persson, K., Bengtson, A., Ceder, G., and Morgan, D. (2006) Ab initio study of the composition dependence of the pressure-induced spin transition in the $(Mg_{1-x},Fe_x)O$ system. Geophysical Research Letters, 33, 1–5.

Pisani, C. (1996) Quantum mechanical ab initio calculation of the properties of crystalline materials, Springer Berlin.

Prencipe, M. (2012) Simulation of vibrational spectra of crystals by ab initio calculations: an invaluable aid in the assignment and interpretation of the Raman signals. Journal of Raman Spectroscopy, in press.

Prencipe, M., Mantovani, L., Tribaudino, L., Bersani, D., and Lottici, P.L. (2012) The Raman spectrum of diopside: a comparison between ab initio calculated and experimentally measured frequencies. European Journal of Mineralogy, in press.

Prencipe, M., Scanavino, I., Nestola, F., Merlini, M., Civalleri, B., Bruno, M., and Dovesi, R. (2011) High-pressure thermo-elastic properties of beryl ($Al_4Be_6Si_{12}O_{36}$) from ab initio calculations, and observations about the source of thermal expansion. Physics and Chemistry of Minerals, 38, 223–239.

Reichmann, H.J., Sinogeikin, S.V., and Bass, J.D. (2008) Single-crystal elastic properties of

$(Mg_{0.987},Fe_{0.013})O$ to 9 GPa. American Mineralogist, 93, 1306–1311.

Robie, R.A., Hemingway, B.S., and Fisher, J.R. (1995) Thermodynamic Properties of Minerals and Related Substances at 298.15 K and 1 Bar (10^5 Pascals) Pressure and at Higher Temperatures. U.S. Geological Survey Bulletin, 2131.

Scanavino, I., Belousov, R., and Prencipe, M. (2012) Ab initio quantum-mechanical study of the effects of the inclusion of iron on thermoelastic and thermodynamic properties of periclase (MgO). Physics and Chemistry of Minerals, 39, 649–663.

Speziale, S., Lee, V.E., Clark, S.M., Lin, J.F., Pasternak, M.P., and Jeanloz, R. (2007) Effects of Fe spin transition on the elasticity of (Mg,Fe)O magnesiowüstites and implications for the seismological properties of the Earth' s lower mantle. Journal of Geophysical Research, 112, B10212.

Speziale, S., Milner, A., Lee, V.E., Clark, S.M., Pasternak, M.P., and Jeanloz, R. (2005) Iron spin transition in Earth's mantle. Proceedings of the National Academy of Sciences of the United States of America, 102, 17918–22.

Sturnhahn, W., Jackson, J.M., Lin, J.F. (2005) The spin state of iron in minerals of Earth's lower mantle. Geophysical Research Letters, 32, L12307

Tsuchiya, T., Wentzcovitch, R.M., da Silva, C., and de Gironcoli, S. (2006) Spin Transition in Magnesiowüstite in Earth's Lower Mantle. Physical Review Letters, 96, 1–4.

Ungureanu, C.G., Cossio, R., and Prencipe, M. (2010) Thermodynamic properties of CaCO3 aragonite at high pressure: An ab-initio quantum-mechanical calculation. European Journal of Mineralogy, 22, 693–701.

Ungureanu, C.G., Cossio, R., and Prencipe, M. (2012) An Ab-initio assessment of thermo-elastic properties of CaCO3 polymorphs: Calcite case. Calphad, 37, 25–33.

Vinet, P., Ferrante, J., Rose, J.H., and Smith, J.R. (1987) Compressibility of solids. Journal of Geophysical Research, 92, 9319–9325.

Vinet, P., Smith, J.R., Ferrante, J., and Rose, J.H. (1987) Temperature effects on the universal equation of state of solids. Physical Review B, 35, 1945–1953.

van Westrenen, W. et al. (2005) Thermoelastic properties of $(Mg_{0.64}Fe_{0.36})O$ ferropericlase based on in situ X-ray diffraction to 26.7GPa and 2173K. Physics of the Earth and Planetary Interiors, 151, 163–176.

Wentzcovitch, R.M., Justo, J.F., Wu, Z., da Silva, C.R.S., Yuen, D.A., and D. Kohlstedt (2009) Anomalous compressibility of ferropericlase throughout the iron spin cross-over. Proceedings of the National Academy of Sciences of the United States of America, 106, 8447-8452.

Wood, B.J. (2000) Phase transformations and partitioning relations in peridotite under lower mantle conditions. Earth and Planetary Science Letters, 174, 341–354.

Wu, Z., and Cohen, R. (2006) More accurate generalized gradient approximation for solids. Physical Review B, 73, 2–7.

Wu, Z., Justo, J., da Silva, C., de Gironcoli, S., and Wentzcovitch, R.M. (2009) Anomalous thermodynamic properties in ferropericlase throughout its spin crossover. Physical Review B, 80, 014409.

Zhang, J., and Kostak, P. (2002) Thermal equation of state of magnesiowüstite $(Mg_{0.6}Fe_{0.4})O$. Physics of the Earth and Planetary Interiors, 129, 301–311.

Zicovich-Wilson, C.M., Pascale, F., Roetti, C., Saunders, V.R., Orlando, R., and Dovesi, R. (2004) Calculation of the vibration frequencies of alpha-quartz: the effect of Hamiltonian and basis set. Journal of computational chemistry, 25, 1873–81.